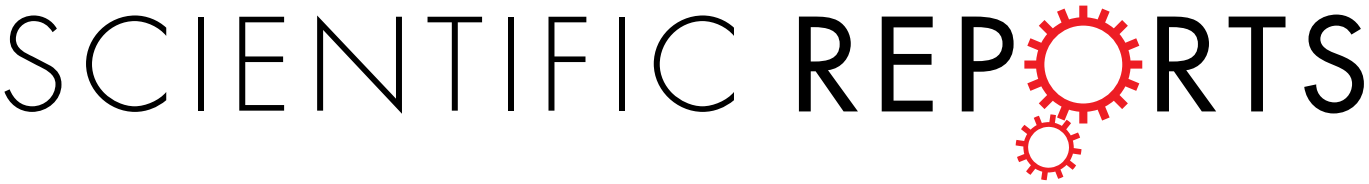

OPEN

Design of Reduction Process of SnO_2 by CH_4 for Efficient Sn Recovery

Received: 30 August 2017
Accepted: 16 October 2017
Published online: 31 October 2017

Hyunwoo Ha[1], Mi Yoo[1], Hyesung An[1], Kihyun Shin[2,4], Taeyang Han[1], Youhan Sohn[1], Sangyeol Kim[1,3], Sang-Ro Lee[3], Jun Hyun Han[1] & Hyun You Kim[1]

We design a novel method for the CH_4 reduction of SnO_2 for the efficient recovery of Sn from SnO_2 through a study combining theory and experiment. The atomic-level process of CH_4-SnO_2 interaction and temperature-dependent reduction behavior of SnO_2 were studied with a combination of a multi-scale computational method of thermodynamic simulations and density functional theory (DFT) calculations. We found that CH_4 was a highly efficient and a versatile reducing agent, as the total reducing power of CH_4 originates from the carbon and hydrogen of CH_4, which sequentially reduce SnO_2. Moreover, as a result of the CH_4 reduction of SnO_2, a mixture of CO and H_2 was produced as a gas-phase product (syngas). The relative molar ratio of the produced gas-phase product was controllable by the reduction temperature and the amount of supplied CH_4. The laboratory-scale experimental study confirmed that CH_4 actively reduces SnO_2, producing 99.34% high-purity Sn and H_2 and CO. Our results present a novel method for an efficient, green, and economical recycling strategy for Sn with economic value added that is held by the co-produced clean energy source (syngas).

Recovering (extracting) metallic elements from ores has occurred throughout human history[1–5]. Advanced copper and iron smelting technology was required for the development of civilization in history[1–5]. However, although dry- or hydro-smelting technologies are currently used as a core technology in industry, many of these technologies are not green or environmentally friendly[6–13]. The most common dry-smelting or reduction of ores by carbon and flux typically byproduces CO_2 and slag at high temperatures[13–15]. In addition, electrolytic smelting or refining of low-quality metal sources is not cost-effective and produces highly corrosive liquid wastes[6–10,16,17]. During the development of human civilization over the past thousands of years, the most easily mineable and accessible high purity ores have been used first due to economic efficiency. The relative depletion of most economically accessible and mineable ores naturally accompanies the accumulation of used metal wastes; many of these wastes are not appropriately recycled.

Sn (Tin) is a highly demanded industrial material[18–22] that is important for the production of electronics[23–26], sensors[27–30], glasses[31–33], and displays[23,34,35]. The industrial demand of Sn is expected to gradually increase in the near future[20–22] as Sn plays as a central role in Pb-free solder[36,37] and transparent electrode[23,34,35]. The current London metal exchange market price of Sn is approximately $19,900/metric ton as of July 2017[38], which is more than 3 and 10 times more expensive than Cu and Al, respectively[38]. However, currently, only approximately 30% of the annual industrially consumed Sn is being recovered worldwide[39], meaning that the remaining 70% of the Sn used is excluded from the recycling process and is eventually wasted. In principle, recovering a metallic element from used metals (wastes and scraps) requires a similar process to the initial ore smelting. To recover high-purity metal from used metal wastes, a combined smelting-electrolytic refining process is typically required, making the recovery process economically nonadvantageous[6,7,9,10,12,13,16]. Such a complicated recovery process weakens the economic driving force for the recovery of metals, such as Sn, which is consumed heavily worldwide.

[1]Department of Materials Science and Engineering, Chungnam National University 99 Daehak-ro, Yuseong-gu, Daejeon, 34134, Republic of Korea. [2]Department of Materials Science and Engineering, KAIST, 291 Daehak-ro, Yuseong-gu, Daejeon, 34141, Korea. [3]A1 Engineering Co.,Ltd., 80-19 Yulchonsandan 1-ro, Haeryong-myeon, Suncheon-si, Jeollanam-do, 58034, Republic of Korea. [4]Present address: Department of Chemistry and the Institute for Computational Engineering and Sciences, University of Texas at Austin, Austin, TX, USA. Hyunwoo Ha, Mi Yoo and Hyesung An contributed equally to this work. Correspondence and requests for materials should be addressed to J.H.H. (email: jhhan@cnu.ac.kr) or H.Y.K. (email: kimhy@cnu.ac.kr)

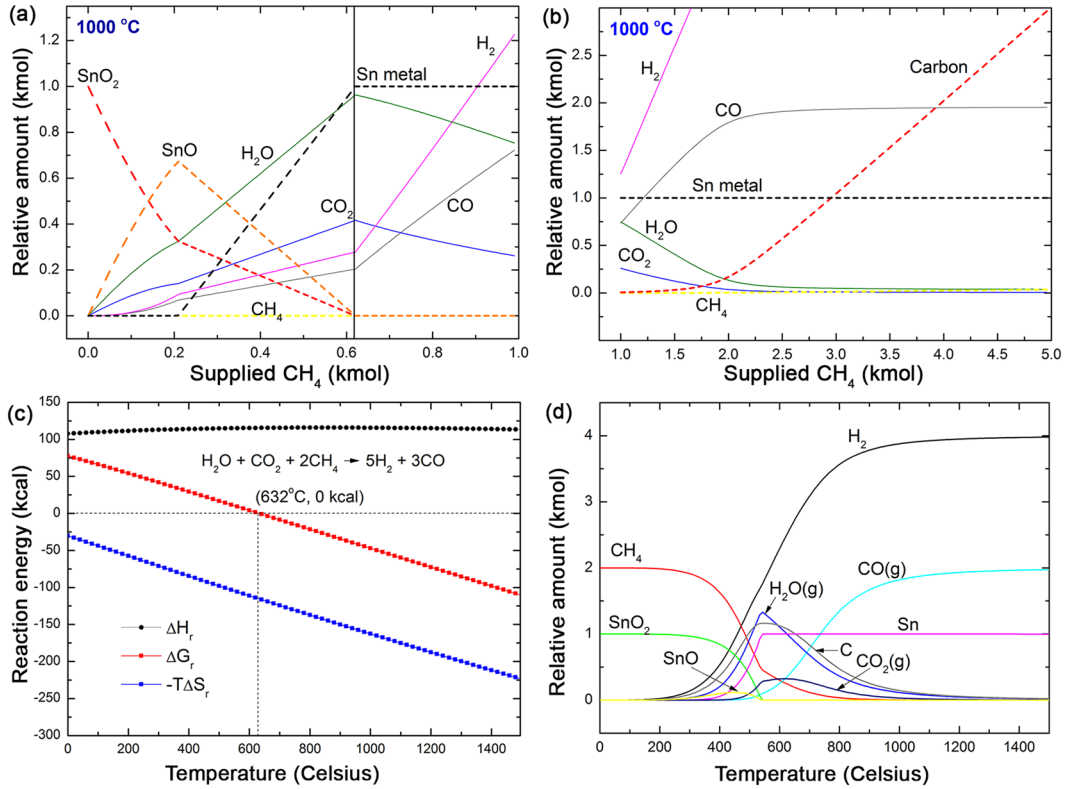

Figure 1. Theoretical prediction of the MR of SnO_2. (**a**,**b**) Equilibrium concentration of the mixture of one kmole of SnO_2 and n·CH_4 ($n = 0$~5, continuously increasing by a step of 0.01 kmole) at 1000 °C as a function of the amount of supplied CH_4. (**a**) $0 \leq n \leq 1.0$, (**b**) between CH_4 and the pre-produced gas-phase products occur as the R ratio exceeds 0.62. (**c**) Temperature dependent reaction energies of two sets of mixtures of gas-phase molecules. The red solid symbols represent the reaction Gibbs free energy, ΔG_r, for $H_2O + CO_2 + 2CH_4 \rightarrow 5H_2 + 3CO$. The gas phase reaction becomes thermodynamically driven at above 632 °C. (**d**) Temperature dependent equilibrium relative concentration of a SnO_2-CH_4 mixture. The initial R value was set to 2.0. Theoretical maximum recovery of Sn was achieved at approximately 550 °C. Although the solid-state reduction of SnO_2 to Sn was completed at 550 °C, the relative concentration of the gas-phase products varies as a function of temperature and converges at approximately 1000 °C.

Hydrogen or methane have been utilized as a reducing agent for metal oxides[40–47]. For example, methane reduction (MR)[41,46] or hydrogen reduction of ZnO[44,48] was proposed to overcome environmental or economical disadvantages of conventional dry-smelting or recovery techniques. To the best of our knowledge, there are few previous reports on the MR of SnO_2. Eroglu and coworkers thermodynamically studied and experimentally demonstrated the feasibility of MR of SnO_2 method[42]. They also utilized methane as a reducing agent of various metal oxides[43,45,49] confirming the strong reducing power of methane. However, detailed atomic scale understanding of MR of SnO_2, which is necessary for optimization of the MR reduction method, is scarce.

In this work, considering the findings of previous studies and combining the widely applied methane dry reforming ($CH_4 + CO_2 \rightarrow 2CO + 2H_2$)[50–53] and the conventional reduction of Sn oxides by carbon ($SnO_x + C \rightarrow Sn + CO_x$), we study a novel, environmentally friendly MR method of SnO_2. We hypothesized that carbon and hydrogen from methane independently and actively reduce SnO_2, making the reduction process highly efficient. Moreover, because our MR method utilizes methane and SnO_2 as a reducer and an oxidizer, respectively, the final gas-phase product naturally involves H_2 and CO. The mixture of H_2 and CO, syngas, can be utilized as a feedstock for further Fisher-Tropsch synthesis[50–53] improving the economic accessibility of our method. Thermodynamic simulations confirmed the availability of the MR of SnO_2 and deduced the optimal operation conditions for efficient Sn recovery and syngas ($H_2 + CO$) production. Density functional theory (DFT) calculations revealed the atomic-level understanding of the process. Subsequent experiments demonstrated that the MR method is very promising for economic and environmentally friendly Sn recovery from SnO_x-containing industrial wastes.

Results

Theoretical prediction of CH_4 reduction of SnO_2. Figure 1a and b present the equilibrium concentrations of the mixture for a kmole of SnO_2 and n·CH_4 ($n = 0$~5, continuously increasing by a step of 0.01 kmole) at 1000 °C as a function of the amount of supplied CH_4. These diagrams were designed to phenomenologically describe the continuous reduction process that occurs inside the reduction furnace in which a certain amount of SnO_2 is exposed to a stream of CH_4. In the early phase of reduction, as the amount of supplied CH_4

increases, SnO_2 was gradually reduced to SnO rather than completely reduced to Sn. At less than R = 0.21 (R = amount of supplied CH_4/amount of initial SnO_2 = 0.21), all the decreasing amount of SnO_2 was reduced to SnO (Fig. 1a). In this early phase, the main gas-phase product was H_2O.

As the amount of supplied CH_4 exceeded R = 0.21, SnO_2 and SnO both began to decreased producing the fully reduced metallic Sn (Fig. 1a). At an equilibrium condition, the supplied SnO_2 can be completely reduced to metallic Sn at R = 0.62. Interestingly, even up to R = 0.62, H_2O was the main gas-phase product. At R = 0.62, almost half the total supplied oxygen content from SnO_2 was taken up by hydrogen (H_2O), and the other half formed CO_2 and CO. In the early phase of reduction at less than R = 0.62, the hydrogen and carbon from CH_4 were independently acting as reducing agents. The solid-state reduction of SnO_2 to SnO and Sn by CH_4 was completed at R = 0.62. Up to this point, the amount of SnO_2 and SnO was gradually decreasing and was finally reduced to metallic Sn.

As the R ratio exceeded 0.62, the gas-phase reactions occurred between the excess CH_4 and the pre-existing H_2, CO, O_2, and H_2O in an oxygen-depleted condition (Fig. 1b). All the oxygen from the SnO_2 was already consumed by the hydrogen or carbon. The temperature dependent reaction Gibbs free energy, ΔG_r, estimated for the reaction $H_2O + CO_2 + 2CH_4 \rightarrow 5H_2 + 3CO$, show that ΔG_r becomes negative over at above 632 °C (Fig. 1c). A negative ΔG_r predicts that if CH_4 is continuously supplied to the system over the equilibrium amount for complete solid-state SnO_2 reduction to Sn (R = 0.62), the formation of H_2 and CO becomes thermodynamically preferred at high temperature. As a result of this gas-phase reaction, a mixture of pre-existing CO_2 and H_2O and excessively supplied CH_4 was converted to H_2 and CO at a high temperature (1,000 °C) (Fig. 1b and c).

Figure 1d shows the temperature dependent equilibrium composition map of a mixture of SnO_2 and CH_4 with R = 2.0. This R value was the critical point where the gas-phase reaction described in Fig. 1c was almost completed. The MR of SnO_2 begins at approximately 300 °C. In the temperature range between 300 °C and 550 °C, the sequential solid-state reduction of SnO_2 to SnO and Sn was completed. As predicted in Fig. 1a and b, the amount of H_2O, CO_2, and solid-state carbon produced were rapidly increased in this temperature range. At greater than 550 °C, the gas-phase reaction described in Fig. 1c drives a redistribution of the gas-phase products. Because R = 2.0 is generally the condition with excess CH_4, a mixture of CH_4, H_2O, and CO_2 naturally transforms to H_2 and CO. Moreover, solid-state carbon began to appear even in the initial phase of the solid-state reduction process due to the presence of excess CH_4 in the reduction system. However, this carbon was also decreasing at temperatures greater than 550 °C at which the solid-state reduction is completed and the gas-phase reaction begins. At approximately 1000 °C, the entire gas-phase product was transformed to a mixture of H_2 and CO, increasing the H_2/CO ratio up to 2.15.

The molecular level process of SnO_2-CH_4 interaction was studied using DFT calculations. The DFT-calculated binding processes of CH_4 on the (100) and (110) facets of the rutile-SnO_2 show that SnO_2 dissociatively binds CH_4, producing a lattice oxygen-bound methyl group (O-CH_3^*) and a surface hydroxyl (-OH^*) (S0 of Fig. 2a and b).

On SnO_2(100) surface (Fig. 2a), the energetics shows that the direct production of H_2O from O-CH_3^* and –OH^* is highly endothermic (ΔE = 1.23 eV) and requires high energy barrier (ΔE_{b1} = 1.52 eV, a panel below the S0 of Fig. 2a). Oh the other hand, further dehydrogenation of O-CH_3^* coupled with the formation of additional -OH^* is more energetically preferred (S1 of Fig. 2a, ΔE = 0.51 eV and ΔE_{b2} = 1.02 eV). We found that, from two separated –OH^* groups, the formation of H_2O molecule is energetically preferred (S2 of Fig. 2) to the H_2 formation (see a panel below S1 of Fig. 2a, ΔE = 1.83 eV) which is again highly endothermic. The desorption of water from the S2 requires only 0.37 eV (see S3 of Fig. 2a). However, further dehydrogenation of O-CH_2^* group is endothermic and requires high barrier of 1.12 eV (S4 of Fig. 2a, ΔE_{b3} = 1.12 eV). Once a O-CH_2^* acetylene group is dissociated, H_2O and CO or CO_2 production follows. Particularly, the preferred formation of H_2O is thermodynamically and kinetically favored to the formation of H_2, confirming the trend in Fig. 1a. Another interesting feature is that a CO molecule was spontaneously formed upon dehydrogenation of a O-CH^* group, as presented in S4 and S5 of Fig. 2a. We also found that this CO molecule directly attacks the surface and be transformed to CO_2 with ΔE of −1.61 eV (S7, Fig. 2a). The processes presented in S5 to S7 suggest that solid carbon could directly reduce SnO_2. However, as the case of carbon coking generally observed in CH_4 reforming catalysis[50–53], sudden deposition of solid carbon may block the surface of SnO_2. However, considering that solid carbon would float on the surface of reduced molten Sn, coking would not be a severe issue in MR of SnO_2.

An almost identical reduction process was observed on SnO_2(110) (Fig. 2b). The notable difference is that the first O-CH_3^* dehydrogenation on SnO_2(110) is relatively slow compared to that on SnO_2(100). Dissociation of a O-CH_2^* described in S3 and S4 is energetically and kinetically similar with that on SnO_2(100). Most importantly, SnO_2(110) surface provides the easier H_2O desorption pathways as presented in S2 and S3 (ΔE = 0.11 eV) and S5 and S6 (ΔE = 0.13 eV). Because several high-index facets could coexist on the surface of SnO_2 particles or powders, we believe that our DFT-generated SnO_2 reduction pathways would proceed in a bi-functional or a multi-functional manner: Dissociation of a O-CH_3^* or a O-CH_2^* groups and formation and desorption of H_2O could occur in a different local area of SnO_2.

From the molecular structure points, the carbon from CH_4 cannot aggressively reduce SnO_2 in the early phase of reduction. The hydrogen atoms of CH_4 reduce Sn oxides first, and the carbon from CH_4 subsequently reduces the Sn oxides.

CH_4 reforming of CO_2 (dry reforming, $CH_4 + CO_2 \rightarrow 2H_2 + 2CO$) and CH_4 steam reforming ($CH_4 + H_2O \rightarrow 3H_2 + CO$) have been applied to produce a mixture of CO and H_2, which is a feedstock for Fisher-Tropsch synthesis. In general, the molar ratio of H_2 and CO in the CH_4 reforming product gas varies between 1 (dry reforming) and 3 (steam reforming)[12,21,39,50]. In Fig. 1a, at less than R = 0.62, H_2 and CO were minority gas-phase products. However, as SnO_2 and SnO are consumed and the gas-phase reactions occur in oxygen-depleted condition between CH_4 and pre-produced gas-phase molecules, the H_2/CO ratio rapidly increases as a function of the amount of supplied CH_4. The rapid increase of the H_2/CO ratio is

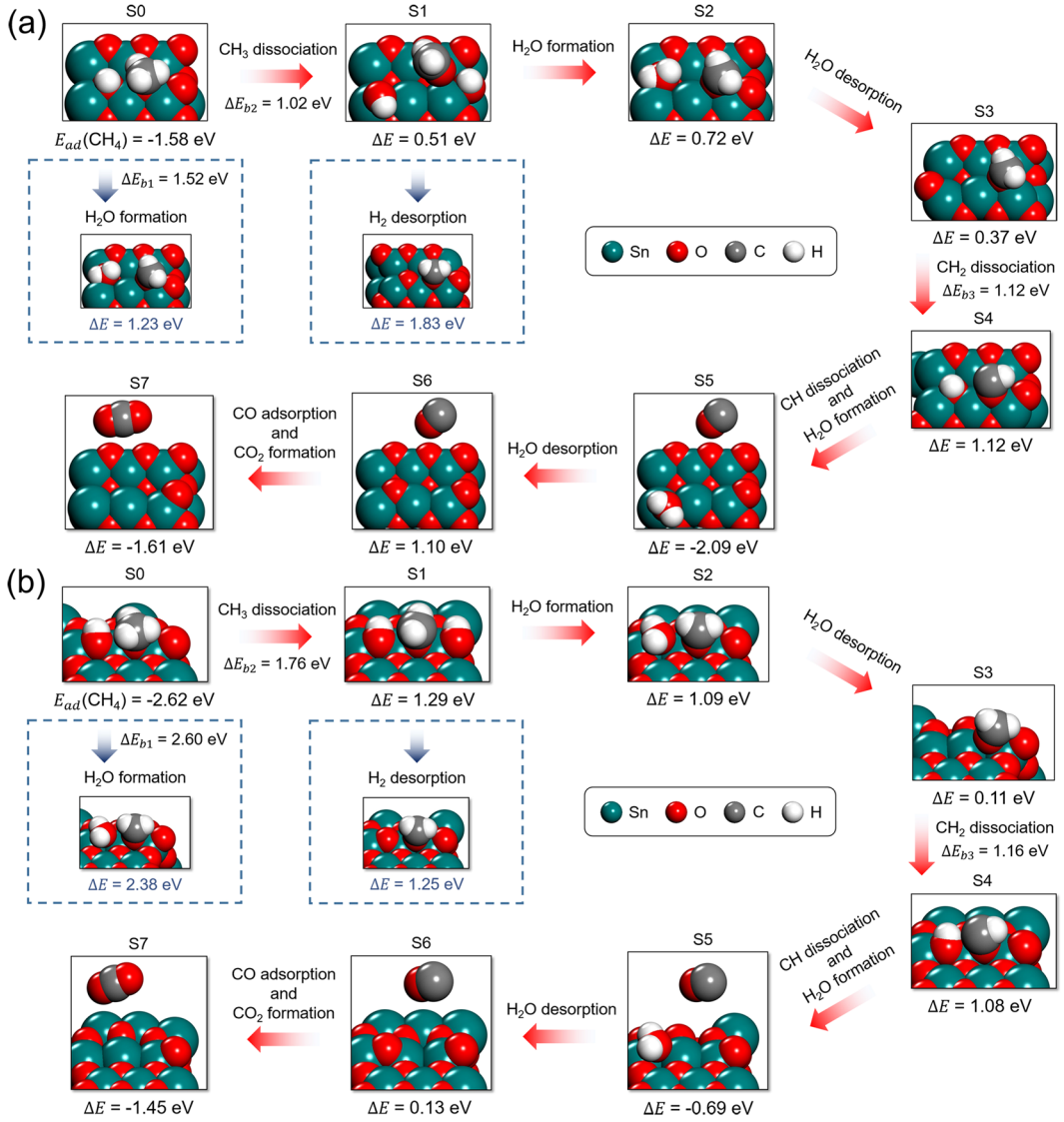

Figure 2. Energetics of SnO_2 reduction by surface-bound CH_4. (**a**) SnO_2 (100) surface. (**b**) SnO_2 (110) surface. On both SnO_2 facets, formation of H_2O was energetically preferred to H_2. The red arrows present the preferred reaction pathway. $E_{ad}(CH_4)$ represents the adsorption energy of CH_4 on the SnO_2 surfaces. ΔE of each step represents the energetic state of the current state relative to the previous state. For example, $\Delta E = 0.51$ eV of S1 in (**a**) means that 0.51 eV of energy is required for CH_3 dissociation from S0 to S1.

phenomenologically feasible because excess CH_4 supplies H, which enters into the system. Moreover, the negative ΔG_r also drives the release of H atoms from H_2O molecules in the form of H_2 molecules.

Typically, CH_4 dry reforming operates at high temperatures above 500 °C and is catalyzed by the transition metal or novel metal catalysts[54,55]. It is not clear whether molten liquid Sn in our system catalyzes the reaction described in Fig. 1c. A recent report by Wetzel and coworkers showed that molten Sn facilitates the thermal dissociation of CH_4 and thus the formation of solid-state carbon and H_2[56,57]. Considering that solid-state carbon and H_2 were increasingly accumulating at greater than R = 2.0 (Fig. 1b), CH_4 dissociation by molten Sn may be attributed to the rapid H_2 and solid carbon formation.

Thermodynamic simulation results presented in Fig. 3 show that the rate of the gas phase reaction, $H_2O + CO_2 + 2CH_4 \rightarrow 5H_2 + 3CO$, does not critically affected by the presence of metallic Sn (or molten Sn, Fig. 3a and b). On the other hand, the addition of metallic Sn promotes thermal decomposition of CH_4 (Fig. 3c and d). At 550 °C, at which the solid-state reduction is completed, the amount of decomposed CH_4 was increased by 19.8 % in the presence of metallic Sn. This result theoretically reproduces the recent experimental findings reported by Wetzel and coworkers[56,57].

Although the MR of SnO_2 is not a catalytic reaction, a reasonable amount of the H_2 and CO mixture was acquired as a byproduct as the R value exceeded 0.62. At approximately R = 2.0, H_2O and CO_2 in the system began to be depleted. All the oxygen in the system was taken by carbon-forming CO molecules, and the excess carbon

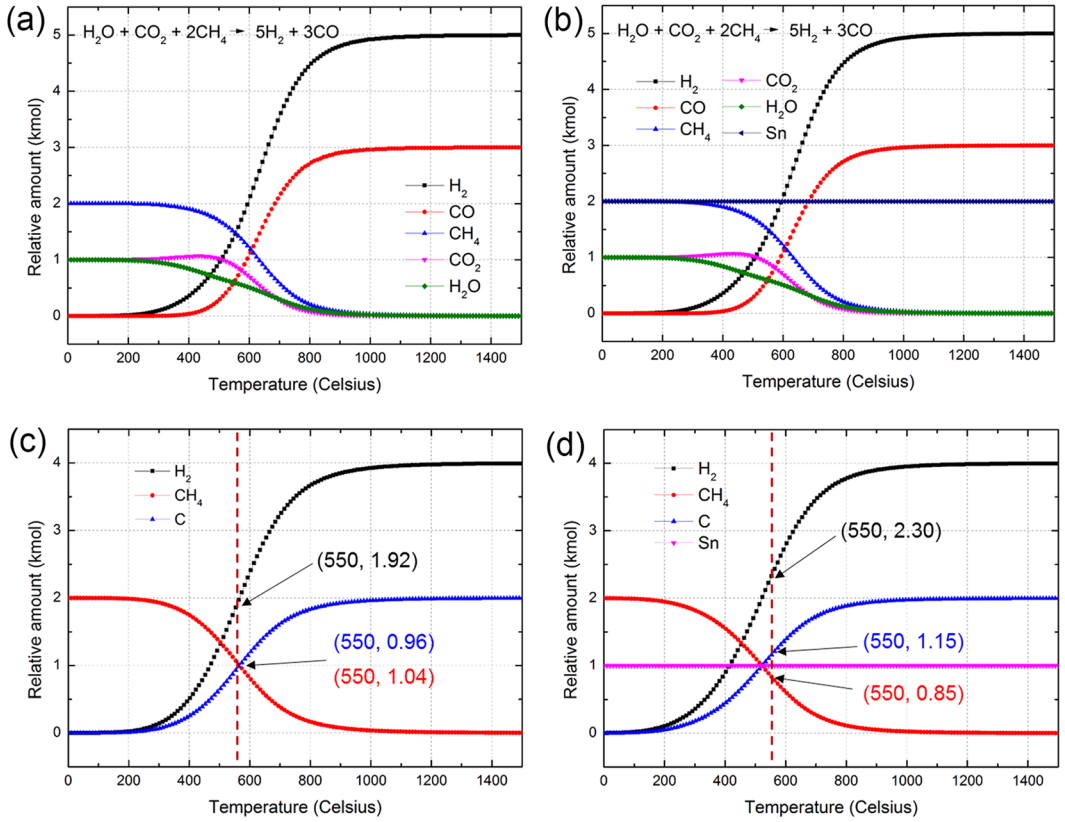

Figure 3. Thermodynamic simulations of the Sn effect on the gas phase reactions. (**a**,**b**) Temperature dependent equilibrium concentration of gas phase species without Sn (**a**) and with Sn (**b**). The presence of metallic Sn does not significantly affect the transformation of $H_2O + CO_2 + 2CH_4$ to $5H_2 + 3CO$. (**c**,**d**) Temperature dependent concentration of CH_4 and decomposed products; H_2 and C, without Sn (**c**) and with Sn (**d**). Metallic Sn accelerates thermal decomposition of CH_4 into C and H_2. The numbers in the parentheses represent the equilibrium concentration of CH_4, C, and H_2 at 550 °C, at which theoretical maximum recovery of Sn was achieved (see Fig. 1d).

from the CH_4 was transformed to solid carbon. During this stage, the increasing H_2 content in the system was entirely from the excess CH_4.

Experimental confirmation of CH_4 reduction of SnO_2. To verify the feasibility of the theoretically proposed concept of the MR of SnO_2, we constructed a laboratory-scale experimental reduction furnace (Figure S1) with continuously flowing CH_4 over the exposed SnO_2 powders. Figure 3a and b show the before and after images of an aluminum boat initially loaded with 25 g of SnO_2 and reduced at 1000 °C with supplied CH_4. Ar-balanced CH_4 gas continuously flowed through a quartz tube furnace for a total reduction time of 1 hour (flow rate of CH_4: 250 sccm). Inevitably, a large portion of supplied CH_4 bypasses SnO_2 powders, being decomposed eventually into C and H_2. Of course, an industrially applicable furnace should be designed to minimize the amount of bypassing CH_4.

The presence of a glittering metallic phase in Fig. 3b shows that SnO_2 was reduced to metallic Sn. An XRD analysis confirmed that initial SnO_2 was reduced to crystalline β-Sn (Fig. 4c). A data set tabulated in Table 1 shows the high purity of the Sn reduced by CH_4. It is remarkable that almost 80% of the supplied Sn was recovered (Fig. 4) even in the test batch experiment. Additionally, the reduced Sn had a high purity of 99.34% (ICP-analyzed). The concentration of the gas phase products shows a high H_2/CO ratio of 5.99, which exceeds the theoretical maximum of conventional CH_4 reforming (Table 2). As we mentioned above, thermally decomposed bypassing CH_4 contributes to the high H_2/CO ratio. The thermodynamically predicted H_2/CO ratio in our reaction condition is about 2.30, which is close to that of convenient syngas for fuel production[58].

Discussion

Development of an environmentally friendly and economically accessible reduction technology for low-quality used metal wastes is key for the sustainable use of limited resources. The MR of SnO_2 method is environmentally and economically novel compared to the conventional dry- and wet-reduction methods, as the MR of SnO_2 does not involve the use of solid reducing agents and liquid-phase acidic electrolytes. The efficiency of the MR of SnO_2 was theoretically proposed and experimentally verified. Moreover, because the MR of SnO_2 occurs at the solid-gas phase interface, the reaction can be more effective than solid-solid interactions of conventional dry reduction.

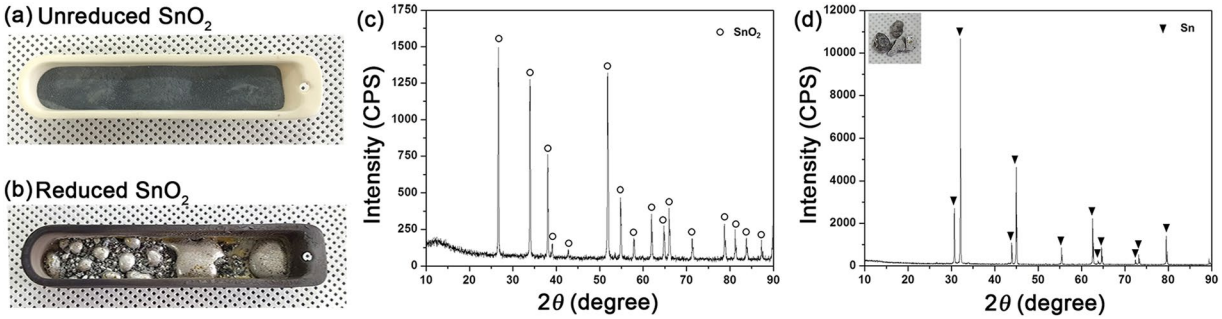

Figure 4. Experimental results of the CH_4 reduction of SnO_2. Photos of unreduced SnO_2 powder (**a**) and CH_4 reduced SnO_2 (**b**). (**c**) and (**d**) show XRD spectra of unreduced SnO_2 and reduced SnO_2, respectively. XRD pattern in (d) demonstrates a typical case of β-Sn. The recovery rate of Sn was 79.9 %.

Element	Sn	Sb	As	Cu	Fe
Composition (at %)	99.34	0.13	0.001	0.49	0.04

Table 1. ICP-analyzed composition of the reduced Sn.

Molecule	H_2[b]	CO[b]	CO_2	CH_4
Concentration (%)	83.9	14.0	1.7	0.4

Table 2. Molecular concentration of the gas-phase product from the CH_4 reduction of SnO_2 analyzed using gas chromatography[a]. [a]H_2O was not analyzed. [b]$H_2/CO = 5.99$.

CH_4 is a quite efficient and versatile reducing agent because the carbon and hydrogen of CH_4 sequentially reduce SnO_2 and produce various gas-phase products. This versatility of CH_4 is highly beneficial for practical uses because the two most representative reducing agents, hydrogen and carbon, contribute to the total reducing power of CH_4.

The theoretical interpretation predicts that as a result of a gas-phase reaction between excess CH_4 and pre-produced H_2O and CO_2, the carbon and hydrogen in the reduction system are eventually transferred to CO and H_2. Our theory-experimental combination study found that the H_2/CO ratio in the gas-phase product is adjustable by controlling the amount of supplied CH_4 and the temperature. Gas-phase reactions between initial gas-phase products of SnO_2 and CH_4 interaction should be considered for optimization of H_2/CO ratio. The economic value added of the MR of SnO_2 increases as long as syngas is producible as a byproduct. Industrially attractable quality of syngas could be produced through further optimization of the reaction temperature, total reaction time, and supplied SnO_2/CH_4 ratio.

In addition, our preliminary calculations show that butane or propane also vigorously reduce SnO_2. For instance, we found that propane completed the SnO_2 reduction at around 400 °C. Considering that the MR of SnO_2 was finished at 550 °C (see Fig. 1c), this preliminary data predicts that the propane reduction of SnO_2 would be economically more effective than the MR of SnO_2. If their reducing power is verified by experiment, more economically accessible liquid natural gas or liquid petroleum gas could be applied for the reduction of SnO_2. As a first step, we are currently working on the optimization of the MR of SnO_2 and the utilization of liquid natural gas for SnO_2 reduction. The relevant results will be reported in due course.

Conclusions

We studied the mechanism of a novel MR of SnO_2 which is a clean, environmentally friendly reduction method for SnO_2. DFT calculations and thermodynamic simulations show that the carbon and hydrogen of CH_4 bound to the surface of SnO_2 independently and sequentially reduce SnO_2. Various gas-phase products, such as H_2O, CO, CO_2, and H_2, were produced from the early phase of reduction. The relative composition of the gas-phase product varies as a function of the amount of supplied CH_4 and the temperature. In the early phase of the MR of SnO_2 (low-temperature or less than $R = 0.62$ of supplied CH_4), hydrogen acts as a dominant reducer. As the supplied CH_4 increases, the carbon from CH_4 aggressively takes the oxygen from H_2O and CO_2 forming CO. Hydrogen from CH_4 and H_2O is released as H_2. The optimized operating condition of 1,000 °C and $R = 2.0$ was suggested from thermodynamic simulation data.

The reliability of this method was confirmed using an experimental batch test performed at 1,000 °C. The high recovery of our MR of SnO_2 (approximately 80%) and the high purity (99.34%) of the reduced Sn demonstrate the novelty of our method.

Our results demonstrate a novel MR method for SnO_2 as an efficient and green method for recovery of Sn from SnO_2. In addition to the reduced metallic Sn, only several gas phase molecules and solid carbon were produced. The H_2/CO ratio in the gas-phase product was controllable by the amount of CH_4 supplied and the operating

temperature. Our results open new avenues for the efficient and economic recovery of highly demanded metallic elements from complex oxide wastes, for example, the recovery of In and Sn from indium-tin oxide.

Methods

Thermodynamic simulations. Thermodynamic simulations were performed with the HSC 6.0 code (Outotec Research, www.hsc-chemistry.com). The relative thermodynamic stability of various Sn, C, O, and H chemical compounds was estimated at temperatures between 0 °C and 1,500 °C. For the initial equilibrium simulation, a mole of SnO_2 was balanced with continuously increasing CH_4 from 0 to 5 moles to clarify the effect of the SnO_2/CH_4 ratio (R) on the relative amount of the final products.

Density functional theory calculations. Quantum chemical DFT calculations were performed with the VASP code[59]. A $3 \times 2 \times 4$ rutile (110) and a $2 \times 3 \times 5$ (100) supercells were used for surface reaction calculations and the most bottom triple layer was fixed during the optimization to ensure the structural robustness of the slab models (refer to Figure S2 for supercell geometry). Electron exchange and correlation were modeled using the Perdew-Burke-Ernzerhof (PBE)[60] functional and the interaction between the ionic cores and the valence electrons was described with the projector augmented-wave method[61]. The valance-electron wave functions were expanded in the plane-wave basis set up to the energy cutoff of 400 eV. The convergence criteria for the electronic structure and the atomic geometry were 10^{-4} eV and 0.03 eV/Å, respectively.

Experimental procedure. A high purity SnO_2 electrode, which was previously used in glass-producing electric furnaces[32], was acquired from Corning precision materials (Gumi, Korea). The average particle diameter of SnO_2 powders was 135 μm (Figure S3). For the laboratory scale MR of SnO_2 experiments, an alumina boat was loaded with 25 g of SnO_2 powder and exposed to a stream of CH_4 and Ar for 1 hour at 1000 °C. The CH_4 flow rate was 250 sccm. The molar ratio of the total supplied CH_4 was 1.85 to SnO_2. The gas-phase concentration and composition of the reduced Sn was analyzed using gas chromatography (GC) and induced coupled plasma (ICP).

Data availability. The datasets generated during and/or analyzed during the current study are available from the corresponding author on reasonable request.

References

1. Photos, E. The question of meteoritic versus smelted nickel-rich iron: Archaeological evidence and experimental results. *World Archaeol.* **20**, 403–421 (1989).
2. Needham, S. P., Leese, M. N., Hook, D. R. & Hughes, M. J. Developments in the Early Bronze Age metallurgy of southern Britain. *World Archaeol.* **20**, 383–402 (1989).
3. Roberts, B. Creating traditions and shaping technologies: understanding the earliest metal objects and metal production in Western Europe. *World Archaeol.* **40**, 354–372 (2008).
4. Radivojević, M. *et al*. On the origins of extractive metallurgy: new evidence from Europe. *J. Archaeol. Sci.* **37**, 2775–2787 (2010).
5. Schmidt, P. & Avery, D. H. Complex Iron Smelting and Prehistoric Culture in Tanzania. *Science* **201**, 1085 (1978).
6. Kang, H. N., Lee, J.-Y. & Kim, J.-Y. Recovery of indium from etching waste by solvent extraction and electrolytic refining. *Hydrometallurgy* **110**, 120–127 (2011).
7. Rimaszeki, G., Kulcsar, T. & Kekesi, T. Application of HCl solutions for recovering the high purity metal from tin scrap by electrorefining. *Hydrometallurgy* **125**, 55–63 (2012).
8. Jun, W. S., Yun, P. S. & Lee, E. C. Leaching behavior of tin from Sn–Fe alloys in sodium hydroxide solutions. *Hydrometallurgy* **73**, 71–80 (2004).
9. Kim, S.-K., Lee, J.-C. & Yoo, K. Leaching of tin from waste Pb-free solder in hydrochloric acid solution with stannic chloride. *Hydrometallurgy* **165**, 143–147 (2016).
10. Lee, M.-S., Ahn, J.-G. & Ahn, J.-W. Recovery of copper, tin and lead from the spent nitric etching solutions of printed circuit board and regeneration of the etching solution. *Hydrometallurgy* **70**, 23–29 (2003).
11. Little, P. & Martin, M. H. A survey of zinc, lead and cadmium in soil and natural vegetation around a smelting complex. *Environ. Pollut. (1970)* **3**, 241–254 (1972).
12. Itoh, S. & Maruyama, K. *High Temp. Mater. Processes* **30**, 317–322 (2011).
13. Rabah, M. A. Combined hydro-pyrometallurgical method for the recovery of high lead/tin/bronze alloy from industrial scrap. *Hydrometallurgy* **47**, 281–295 (1998).
14. Sripriya, R. & Murty, C. V. G. K. Recovery of metal from slag/mixed metal generated in ferroalloy plants—a case study. *Int. J. Miner. Process.* **75**, 123–134 (2005).
15. Mitchell, A. R. & Parker, R. H. The reduction of SnO_2 and Fe_2O_3 by solid carbon. *Miner. Eng.* **1**, 53–66 (1988).
16. Li, Y., Liu, Z., Li, Q., Liu, Z. & Zeng, L. Recovery of indium from used indium–tin oxide (ITO) targets. *Hydrometallurgy* **105**, 207–212 (2011).
17. Gupta, B., Mudhar, N. & Singh, I. Separations and recovery of indium and gallium using bis(2,4,4-trimethylpentyl)phosphinic acid (Cyanex 272). *Sep. Purif. Technol.* **57**, 294–303 (2007).
18. Thoburn, J. T. *Tin in the world economy*. (Edinburgh University Press, 1994).
19. François Hennart, J. Upstream vertical integration in the aluminum and tin industries. *J. Econ. Behav. Organ.* **9**, 281–299 (1988).
20. https://www.itri.co.uk/sustainability/news-5/itri-survey-tin-demand-growing-slowly.
21. https://www.itri.co.uk/information/tinplate/general/tin-for-tomorrow-contributing-to-global-sustainable-development.
22. https://www.itri.co.uk/market-analysis/consumption/itri-survey-shows-tin-use-stable-to-slightly-stronger-in- (2016).
23. Bae, J.-Y., Park, J., Kim, H. Y., Kim, H.-S. & Park, J.-S. Facile Route to the Controlled Synthesis of Tetragonal and Orthorhombic SnO_2 Films by Mist Chemical Vapor Deposition. *ACS Appl. Mater. Inter.* **7**, 12074–12079 (2015).
24. Snaith, H. J. & Ducati, C. SnO_2-Based Dye-Sensitized Hybrid Solar Cells Exhibiting Near Unity Absorbed Photon-to-Electron Conversion Efficiency. *Nano Lett.* **10**, 1259–1265 (2010).
25. Vilà, A., Gomez, A., Portilla, L. & Morante, J. R. Influence of In and Ga additives onto SnO_2 inkjet-printed semiconductor. *Thin Solid Films* **553**, 118–122 (2014).
26. Kim, H. *et al*. Electrical, optical, and structural properties of indium–tin–oxide thin films for organic light-emitting devices. *J. Appl. Phys.* **86**, 6451–6461 (1999).
27. Bai, S. *et al*. Synthesis of SnO_2–CuO heterojunction using electrospinning and application in detecting of CO. *Sens. Actuators, B* **226**, 96–103 (2016).

28. Suehle, J. S., Cavicchi, R. E., Gaitan, M. & Semancik, S. Tin oxide gas sensor fabricated using CMOS micro-hotplates and *in-situ* processing. *IEEE Electron Device Lett.* **14**, 118–120 (1993).
29. Nayral, C. *et al*. A Novel Mechanism for the Synthesis of Tin/Tin Oxide Nanoparticles of Low Size Dispersion and of Nanostructured SnO_2 for the Sensitive Layers of Gas Sensors. *Adv. Mater.* **11**, 61–63 (1999).
30. Dattoli, E. N., Davydov, A. V. & Benkstein, K. D. Tin oxide nanowire sensor with integrated temperature and gate control for multi-gas recognition. *Nanoscale* **4**, 1760–1769 (2012).
31. Bickerstaff, K. & B, P. L. A. Manufacture of flat glass. US patents: US2911759A (1959).
32. Citti, O., Williams, J. A. A. & McGarry, C. N. Tin oxide material with improved electrical properties for glass melting. US Patents: US7685843B2, (2010).
33. Fourcade, J. & Citti, O. In *73rd Conference on Glass Problems* 183–199 (John Wiley & Sons, Inc., 2013).
34. Betz, U., Kharrazi Olsson, M., Marthy, J., Escolá, M. F. & Atamny, F. Thin films engineering of indium tin oxide: Large area flat panel displays application. *Surf. Coat. Technol.* **200**, 5751–5759 (2006).
35. Ginley, D. S. & Bright, C. Transparent conducting oxides. *MRS Bull.* **25**, 15–18 (2000).
36. Nah, J.-W., Kim, J. H., Lee, H. M. & Paik, K.-W. Electromigration in flip chip solder bump of 97Pb–3Sn/37Pb–63Sn combination structure. *Acta Mater.* **52**, 129–136 (2004).
37. Cho, M. G., Kim, H. Y., Seo, S.-K. & Lee, H. M. Enhancement of heterogeneous nucleation of β-Sn phases in Sn-rich solders by adding minor alloying elements with hexagonal closed packed structures. *Appl. Phys. Lett.* **95**, 021905 (2009).
38. https://www.lme.com.
39. https://www.itri.co.uk/sustainability/material-flow-and-recycling.
40. Khoshandam, B., Jamshidi, E. & Kumar, R. Reduction of cobalt oxide with methane. *Metall. Mater. Trans. B* **35**, 825–828 (2004).
41. Ale Ebrahim, H. & Jamshidi, E. Kinetic Study of Zinc Oxide Reduction by Methane. *Chem. Eng. Res. Des.* **79**, 62–70 (2001).
42. Cetinkaya, S. & Eroglu, S. Thermodynamic analysis and reduction of tin oxide with methane. *Int. J. Miner. Process.* **110**, 71–73 (2012).
43. Cetinkaya, S. & Eroglu, S. Thermodynamic analysis and reduction of tungsten trioxide using methane. *Int. J. Refract. Met. Hard Mater.* **51**, 137–140 (2015).
44. Lee, T.-H. *et al*. Reduction Kinetics of Zinc Powder from Brass Converter Slag by Pyrometallurgical Method Using Hydrogen Gas. *KONA Powder Part. J.* **33**, 278–286 (2016).
45. Altay, M. C. & Eroglu, S. Isothermal Reaction of NiO Powder with Undiluted CH_4 at 1000 K to 1300 K (727°C to 1027°C). *Metal. Mater. Trans. B* **48**, 2067–2076 (2017).
46. Ale Ebrahim, H. & Jamshidi, E. Effect of mass transfer and bulk flow on the zinc oxide reduction by methane. *Ind. Eng. Chem. Res.* **41**, 2630–2636 (2002).
47. Ale Ebrahim, H. & Jamshidi, E. Kinetic Study and Mathematical Modeling of the Reduction of ZnO−PbO Mixtures by Methane. *Ind. Eng. Chem. Res.* **44**, 495–504 (2005).
48. Ng, K. S. *et al*. A multilevel sustainability analysis of zinc recovery from wastes. *Resour. Conserv. Recy.* **113**, 88–105 (2016).
49. Cetinkaya, S. & Eroglu, S. A Single-Step Process for Direct Reduction of Iron Oxide to Sponge Iron by Undiluted Methane. *JOM* **69**, 993–998 (2017).
50. Kim, H. Y., Park, J. N., Henkelman, G. & Kim, J. M. Design of a Highly Nanodispersed Pd–MgO/SiO_2 Composite Catalyst with Multifunctional Activity for CH_4 Reforming. *ChemSusChem* **5**, 1474–1481 (2012).
51. Van Hook, J. P. Methane-Steam Reforming. *Catal. Rev.* **21**, 1–51 (1980).
52. Bradford, M. C. J. & Vannice, M. A. CO_2 Reforming of CH_4. *Catal. Rev.* **41**, 1–42 (1999).
53. Fan, M.-S., Abdullah, A. Z. & Bhatia, S. Catalytic Technology for Carbon Dioxide Reforming of Methane to Synthesis Gas. *ChemCatChem* **1**, 192–208 (2009).
54. Pakhare, D. & Spivey, J. A review of dry (CO_2) reforming of methane over noble metal catalysts. *Chem. Soc. Rev.* **43**, 7813–7837 (2014).
55. Wang, S., Lu, G. Q. & Millar, G. J. Carbon Dioxide Reforming of Methane To Produce Synthesis Gas over Metal-Supported Catalysts: State of the Art. *Energy Fuels* **10**, 896–904 (1996).
56. Abánades, A. *et al*. Development of methane decarbonisation based on liquid metal technology for CO_2-free production of hydrogen. *Int. J. Hydrogen Energy* **41**, 8159–8167 (2016).
57. Geißler, T. *et al*. Hydrogen production via methane pyrolysis in a liquid metal bubble column reactor with a packed bed. *Chem. Eng. J.* **299**, 192–200 (2016).
58. Van Der Laan, G. P. & Beenackers, A. A. C. M. Kinetics and Selectivity of the Fischer–Tropsch Synthesis: A Literature Review. *Catal. Rev.* **41**, 255–318 (1999).
59. Kresse, G. & Furthmuller, J. Efficiency of ab-initio total energy calculations for metals and semiconductors using a plane-wave basis set. *Comput. Mater. Sci.* **6**, 15–50 (1996).
60. Perdew, J. P., Burke, K. & Ernzerhof, M. Generalized gradient approximation made simple. *Phy. Rev. Lett.* **77**, 3865–3868 (1996).
61. Blochl, P. E. Projector Augmented-Wave Method. *Phys. Rev. B* **50**, 17953–17979 (1994).

Acknowledgements

This work was supported by the Korea Institute of Energy Technology Evaluation and Planning (KETEP) and the Ministry of Trade, Industry & Energy (MOTIE) of the Republic of Korea (No. 20155020101050). This research used resources of the Center for Functional Nanomaterials, which is a U.S. DOE Office of Science Facility, at Brookhaven National Laboratory under Contract No. DE-SC0012704. Computing time was provided by the National Institute of Supercomputing and Network/Korea Institute of Science and Technology Information (KSC-2016-C3-0037).

Author Contributions

H.Y.K., J.H.H., and S.-R.L. designed this work. H.H., M.Y., H.A., and K.S. performed thermodynamic simulations and DFT calculations. T.H., Y.S., and S.K. carried out the experiments. H.Y.K. wrote the manuscript. All the authors contributed to discuss on the manuscript.

Additional Information

Supplementary information accompanies this paper at https://doi.org/10.1038/s41598-017-14826-7.

Competing Interests: The authors declare that they have no competing interests.

Publisher's note: Springer Nature remains neutral with regard to jurisdictional claims in published maps and institutional affiliations.